Biophysical Journal
Article

Biophysical Society

Cryo-EM and Molecular Docking Shows Myosin Loop 4 Contacts Actin and Tropomyosin on Thin Filaments

Matthew H. Doran,[1] Elumalai Pavadai,[1] Michael J. Rynkiewicz,[1] Jonathan Walklate,[2] Esther Bullitt,[1] Jeffrey R. Moore,[3] Michael Regnier,[4] Michael A. Geeves,[2] and William Lehman[1,*]

[1]Department of Physiology & Biophysics, Boston University School of Medicine, Boston, Massachusetts; [2]School of Biosciences, University of Kent, Canterbury, Kent, United Kingdom; [3]Department of Biological Sciences, University of Massachusetts-Lowell, Lowell, Massachusetts; and [4]Department of Bioengineering, University of Washington, Seattle, Washington

ABSTRACT The motor protein myosin drives muscle and nonmuscle motility by binding to and moving along actin of thin filaments. Myosin binding to actin also modulates interactions of the regulatory protein, tropomyosin, on thin filaments, and conversely tropomyosin affects myosin binding to actin. Insight into this reciprocity will facilitate a molecular level elucidation of tropomyosin regulation of myosin interaction with actin in muscle contraction, and in turn, promote better understanding of nonmuscle cell motility. Indeed, experimental approaches such as fiber diffraction, cryoelectron microscopy, and three-dimensional reconstruction have long been used to define regulatory interaction of tropomyosin and myosin on actin at a structural level. However, their limited resolution has not proven sufficient to determine tropomyosin and myosin contacts at an atomic-level and thus to fully substantiate possible functional contributions. To overcome this deficiency, we have followed a hybrid approach by performing new cryogenic electron microscopy reconstruction of myosin-S1-decorated F-actin-tropomyosin together with atomic scale protein-protein docking of tropomyosin to the EM models. Here, cryo-EM data were derived from filaments reconstituted with α1-actin, cardiac $\alpha\alpha$-tropomyosin, and masseter muscle β-myosin complexes; masseter myosin, which shares sequence identity with β-cardiac myosin-heavy chain, was used because of its stability in vitro. The data were used to build an atomic model of the tropomyosin cable that fits onto the actin filament between the tip of the myosin head and a cleft on the innermost edge of actin subunits. The docking and atomic scale fitting showed multiple discrete interactions of myosin loop 4 and acidic residues on successive 39–42 residue-long tropomyosin pseudorepeats. The contacts between S1 and tropomyosin on actin appear to compete with and displace ones normally found between actin and tropomyosin on myosin-free thin filaments in relaxed muscle, thus restructuring the filament during myosin-induced activation.

SIGNIFICANCE Mutations in sarcomeric proteins, including mutations detected in actin, tropomyosin, and myosin, are linked to cardiomyopathies and skeletal muscle disease. However, the mechanisms underlying their impact on contraction and relaxation remains unclear because corresponding perturbation of myofilament structure is incompletely defined. In this study, cryoelectron microscopy and protein-protein docking provide a view of tropomyosin-myosin contacts on actin filaments. These interactions are significant in switching between muscle-on and -off states. Indeed, disease-rendering mutations that target such interactions may destabilize the contraction/relaxation cycle. Thus, our results provide a framework for the connection between such molecular insults and pathological progression.

INTRODUCTION

During muscle contraction, myosin-motors that project from thick filaments bind to and move along thin filaments formed from filamentous actin (F-actin). To generate requisite force on the actin-based thin filaments for muscle contraction, myosin heads undergo a power stroke, coupled to ATP hydrolysis and product release. In striated muscles, this process is controlled by the regulatory proteins tropomyosin and troponin located on the surface of the actin filaments. The regulatory proteins provide an on-off switching mechanism to control myosin-mediated motility and consequently muscle activity (1–4). The troponin complex, responding to varied sarcoplasmic Ca^{2+} levels, as well as

Submitted May 29, 2020, and accepted for publication July 7, 2020.

*Correspondence: wlehman@bu.edu

Editor: David Thomas.

https://doi.org/10.1016/j.bpj.2020.07.006

myosin-binding itself, bias tropomyosin to occupy one of three distinct regulatory conformations on the actin surface. This involves a steric reconfiguration of the tropomyosin head-to-tail cable to either hinder access or expose myosin-binding sites on actin and thus govern myosin's interactions with thin filaments and its motor activity (1–4). At low Ca^{2+} levels, troponin-I of the troponin complex constrains tropomyosin coiled coils in a "blocked B-state," in which tropomyosin obstructs myosin-binding to actin, keeping muscle relaxed. With rising Ca^{2+} levels during muscle activation, Ca^{2+}-occupied troponin-C promotes a "C-state," in which myosin-binding sites remain partially "closed" but allow weak myosin-binding. Myosin gaining access to actin then "traps" tropomyosins in an otherwise energetically unfavorable "open M-state" position on actin, resulting in strong myosin-binding and actin-activation of the myosin ATPase. Hence, it follows that tropomyosin movement from its C-location into a fully active M-state position on actin requires myosin participation (1–4). Interestingly, cross-linking studies suggest direct myosin-tropomyosin interaction is possible (5–7). Thus, myosin does not solely function as a molecular motor during contraction but also acts as a modulator of tropomyosin function, and in many muscles, recruitment of myosin from the surface of the thick filaments also influences activity.

The involvement of troponin in tropomyosin-linked control of thin filament behavior has been investigated in much detail over the past 50 years (reviewed in (3)). By contrast, less is known about regulatory reconfiguration of tropomyosin once myosin binds to thin filaments, particularly when considered from a residue-by-residue structural perspective. For example, it is unclear how myosin displaces tropomyosin from its closed-state position into a default open state (8–12). As part of this process, attractive and/or repulsive intermolecular chemical forces between myosin and tropomyosin may facilitate the requisite tropomyosin movement. Myosin-tropomyosin interaction, coupled to strong myosin-actin attachment during the cross-bridge cycle is likely to either "push," "drag" or "chase," and then trap tropomyosin into the open state. Although cryogenic electron microscopy (cryo-EM) studies by the Raunser, Fujii, and Namba laboratories (10–12) showed that loop 4 at the tip of the open-state myosin head appears to restrain tropomyosin topologically against a ridge on the extreme inner edge of actin subdomain 3, any further open-state stabilization by myosin-tropomyosin interactions or by actin conformational dynamics is uncertain (10–13).

In this study, we revisit the structure of M-state thin filaments and address current uncertainties related to myosin-tropomyosin interactions on thin filaments. We define the structure of the myosin motor head on actin-tropomyosin filaments by first performing moderate 4.2 Å resolution cryo-EM of actin-tropomyosin "decorated" with β-myosin subfragment 1 (S1), i.e., with motor heads proteolytically cleaved from full-length myosin. We next apply high-specificity protein-protein-docking protocols to define residue-to-residue contacts made between components and then merge the results of the two methods. We demonstrate periodic interaction between myosin and tropomyosin and provide a more complete paradigm in which myosin-S1 steers tropomyosin away from its default weak C-state interactions with actin subunits along the thin filament, in turn trapping tropomyosin into the M-state position.

Strategy and workflow

The first step in our approach to determine M-state S1-tropomyosin interaction was to generate a three-dimensional (3D) cryo-EM reconstruction of β-myosin-S1-decorated actin-tropomyosin filaments. The objective was to use the reconstruction as a template to fit crystal structures of the filament constituents to generate a hybrid map at high resolution (Fig. 1). Like all recently published cryo-EM structures (10–12,14,15), a 3–6 Å resolution for actin and S1 is sufficient to match corresponding crystal structures of actin and S1 to densities within these maps (Fig. 1). In our work, tropomyosin resolves as an extremely well-defined coiled coil, yet, like in previous reports (8–12,14,15), the coiled coil lacks sufficient surface detail or marked asymmetries to readily define the residue-to-residue register of the coiled coil relative to actin and S1. Thus, additional steps were required to determine residue-level longitudinal positioning and rotation of tropomyosin within the EM volume. Here, the programs PIPER and ClusPro (16–18) were used as computational tools to dock relatively short segments of tropomyosin as ligands to the 4.2 Å resolution actin-S1 model defined by our reconstructions. The docking protocol itself is based on shape complementarity and coiled coil polarity as well as residue-to-residue electrostatic and van der Waals chemical potential. The procedure produced a series of two actin-long acto-S1 cassettes containing tropomyosin fragments that matched respective densities in the EM reconstruction closely, i.e., now the hybrid map contained residue-level tropomyosin assignments in addition to those of actin and S1. The individual cassettes then were stitched together to construct a pseudoatomic model of the M-state filament containing actin, tropomyosin, and S1 components. The composite map was then subjected to energy minimization and molecular dynamics as a means of further refinement (18). It is worth noting that our structural analysis, like that in (12), relied on actin, tropomyosin, and S1 isoforms with sequences found in mammalian muscle.

MATERIALS AND METHODS

Proteins used to reconstitute thin filaments

Myosin

β-Myosin was isolated from bovine masseter muscle tissue and S1 then prepared as described in (19). Bovine masseter muscle contains Type 1 slow

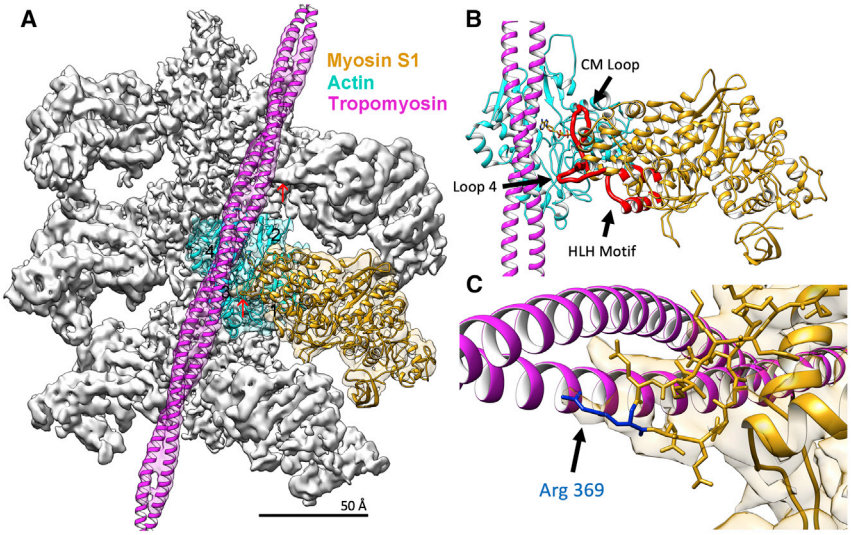

FIGURE 1 Cryo-EM reconstruction of S1-decorated actin-tropomyosin filaments. (*A*) Isosurface rendering of the reconstruction showing atomic models of actin (*cyan*), myosin (*gold*), and tropomyosin (*magenta*) fitted into respective EM densities as described in the Materials and Methods. The pointed end of the filament is facing up; actin subdomains numbered on central actin subunit. Each region of the reconstruction was low-pass filtered to provide better visualization; actin to 4.0 Å, myosin to 5.5 Å, and tropomyosin to 6.5 Å according to local resolution estimates (see Fig. S2). (*B*) Atomic model of the actin-myosin-tropomyosin complex highlighting the actin-myosin interface. Extensive interactions are formed between actin and the myosin cardiomyopathy loop (CM Loop), loop 4, and the helix-loop-helix (HLH) motif (each highlighted in *red*). ADP bound to actin is shown. The residue-to-residue contacts between actin and myosin are tabulated in Table S3. (*C*) Myosin-tropomyosin interaction is visible at myosin loop 4. The cryo-EM density of this region is well resolved, allowing identification of interacting amino acid side chains of myosin, including that of conserved residue Arg369 (*blue*) making contact with the tropomyosin coil-coil (also noted by *red arrows* in (*A*)). To see this figure in color, go online.

muscle myosin. In mammals, slow muscle myosin and β-cardiac myosin, the major cardiac muscle isoform, are the same. They are the products of one gene, *MyHC7*, and have identical heavy chains. The human and bovine isoforms have 96% sequence identity in the motor domain. In the current studies, masseter myosin served as a surrogate for its human cardiac muscle β-myosin counterpart, which is of particular interest because of its dysfunction in many cardiomyopathies. Although these two myosins share virtually identical heavy chains, the isolated and purified masseter myosin and its S1 fragment, unlike the cardiac counterparts, are stable under standard experimental conditions. The masseter S1 can be lyophilized and stored in the presence of 1% (w/v) sucrose before use without loss of activity (19). Also note that loop 4 of mammalian myosin II is highly conserved (see Table S1).

Tropomyosin

Human cardiac α-tropomyosin (Tpm 1.1, also present in significant amounts in skeletal muscles), containing the N-terminal extension Met-Ala-Ser, was expressed and purified as previously (20).

Actin

Skeletal muscle F-actin was prepared by standard methods (21) and used because of its resistance to depolymerization at the low concentrations needed for cryo-EM work; it and cardiac muscle F-actin share the same sequence with conservative substitutions involving four residues.

Sample preparation for cryo-EM

Thin filaments were reconstituted by first mixing F-actin and tropomyosin to final concentrations of 10 μM actin and 7 μM tropomyosin in a buffer consisting 50 mM sodium acetate, 3 mM $MgCl_2$, 1 mM dithiothreitol, 10 mM HEPES buffer at pH 7.0 in a temperature-controlled room at 25°C. We found it essential to replace previously used NaCl or KCl (8) with sodium acetate to prevent tropomyosin dissociation from filaments under cryo-EM conditions. The buffers used throughout preparation were nucleotide-free to maintain "rigor-state" conditions. Excess of tropomyosin was used relative to actin (5:7 mol/mol), rather than a native 1:7 ratio stoichiometry, to ensure full filament saturation. (Although the excess tropomyosin remains unbound, it does not cause noticeable background interference during EM image processing.) Just before applying 1.5 μL actin-tropomyosin to a freshly glow discharged holey-carbon copper grid surface (200 mesh, Quantifoil 2/1; Electron Microscopy Sciences, Hatfield, PA), the surfactant octyl β-D-glucopyranoside (Sigma-Aldrich, St. Louis, MO) was added to the protein solution to a concentration of 12 nM. This facilitated even filament spreading and limited filament adsorption to the air-water interface (22). The grid sample was manually blotted for 1 s at 10°C and 100% humidity, and a 1.5-μL drop of 7.5 μM myosin-S1 subfragment was then applied to the blotted grid sample. The sample was immediately blotted for 4 s and plunge-frozen in liquid ethane using a Vitrobot Mark III system (FEI/Thermo Fisher Scientific, Hillsboro, OR).

Cryo-EM data collection and processing

Samples were examined with a Titan Krios cryo-EM (Thermo Fisher Scientific, Hillsboro, OR) at the Stanford Linear Accelerator Center-National Center for Macromolecular Imaging Cryo-EM facilities (Menlo Park, CA). Micrographs were collected at a magnification of ×130,000 using a 20-eV energy filter. Movies were recorded with a Gatan K2 Summit direct electron detector (Gatan/AMETEK, Berwyn, PA) with each of 35 sequential 0.2 s exposures captured at a dose of 7.5 $e^{-}/Å^2/s$, a defocus of 1.5–2.5 μm and with a pixel size of 1.06 Å. Movie frames were aligned and summed to produce 2496 individual micrographs.

Micrographs were screened to remove images judged to have thick or mottled ice, bundled filaments, or background interference. Image reconstruction was carried out using the RELION 3.0.7 suite of programs, as described by Scheres (23–25). Briefly, micrographs were first motion corrected using MotioCorr2 and the contrast transfer function (CTF) estimated and normalized by the CtfFind4 subroutines in RELION. Filaments were manually selected and divided into 270 Å long (256 pixels) overlapping segments, each offset by 27.5 Å (90% overlap), and 45,040 segments were extracted from 702 micrographs within the original data. Filament segments were then sorted using reference-free two-dimensional classification. Noisy or empty classes were discarded, resulting in 40,455 segments for processing. To further reduce the number of poorly defined segments to be reconstructed, three-dimensional classification was performed, and class averages inspected for quality, here applying F-actin helical symmetry (166.4° subunit rotation around the F-actin helical axis and a subunit axial translation of 27.5 Å). A final set of 32,158 segments was taken for a preliminary three-dimensional refinement by first aligning these particles to a featureless 200-Å diameter cylinder while applying the above helical parameters. The resulting model generated was low pass filtered to be used as a new reference for a second refinement with a smaller angular sampling of view orientations (3.7°) and incorporating a solvent mask to produce an

initial reconstruction at 6.4 Å. We then performed two iterations of CTF refinement and Bayesian "Polishing" (i.e., further electron beam-induced motion correction). Particles underwent CTF refinement with beam tilt estimation and a subset of these particles was evaluated to find optimal polishing parameters. Particles having undergone Bayesian polishing were used in an autorefine run using the 6.4 Å reconstruction, low pass filtered to 60 Å, as a starting model. We additionally employed a soft 6 actin-6 myosin-tropomyosin mask after each iteration to focus the refinement on the central section of the acto-S1 filaments. Our soft solvent mask was created by fitting atomic models of actin, β-myosin-S1, and tropomyosin into the 6.4 Å reconstruction, converting the pdb into an MRC map using the EMAN2 pdb2mrc command (26), and then constructing a mask from this map in RELION. After 24 iterations, this process resulted in a 4.9 Å resolution map (data not shown). The same process was repeated once more to produce a final 4.2 Å resolution map. Further iterations did not improve the resolution. Default processing parameters were used except as noted above. Resolution estimation was made using Fourier shell correlation criteria, $FSC_{0.143}$, in RELION. (See Figs. S1 and S2; Table S2).

All figures were rendered using UCSF Chimera (27).

Acto-S1 model building

The cryo-EM reconstruction served as a template to build an atomic model of the acto-S1 structure in the rigor state. Using the "Fit In Map" subroutine in UCSF Chimera (27), an F-actin structure taken from the Yamada et al. map (15) (Protein Data Bank, PDB: 6KN8) fitted within its corresponding density of the masseter S1-decorated actin-tropomyosin reconstruction. The von der Ecken actin maps (11,14) (PDB: 5JLH and PDB: 5KLF) also fitted in the volume without any notable difference. It would have been ideal to also directly match the volume of myosin in the reconstruction with a crystal structure of striated muscle S1 and then merge it with the actin fitted in the map. However, there is no complementary high-resolution model of striated muscle "rigor-state" S1, nor structures of the β-cardiac or masseter muscle myosin protein available that are nucleotide-free. Therefore, we built a homology model of the β-myosin-S1 based on the rigor-state crystal structure of the squid muscle myosin-S1 (28) (PDB: 3I5G) (as done previously by Fujii and Namba (12) for the same purpose), here replacing squid residues with corresponding residues in the bovine amino acid sequence (UniProt: Q9BE39). To accomplish this, the SWISS-MODEL suite of programs (29) was used to build the bovine masseter β-myosin-S1 model. Please note that we use the bovine β-myosin sequence numbering throughout the text and in the Supporting Material. The homology model then was fitted to the cryo-EM map using the Fit In Map subroutine in UCSF Chimera (27). The vast majority of Cα-chains in the myosin-S1 motor domain, ranging from residues 216 to 624, matched densities visible in the reconstruction. Myosin loop 1 residues 199–216 and loop 2 residues 624–641 located at the distal ends of the reconstructed S1 were removed from the model because of the lack of definitive density for fitting to these regions. Loop 4 (amino acids 354–380) which varies between muscle and nonmuscle sarcomeric myosins 2, but conserved among muscle myosins (see Table S1) was replaced by the corresponding motif of β-cardiac myosin solved in a post-rigor state (30) (PDB: 6FSA). We then refined the models using flexible fitting routines by employing the MDFF routine in the program VMD (31,32), while implementing two plugins, Chirality and Cispeptide, in VMD to prevent possible stereochemical errors and/or overfitting. Each residue in the actin and β-myosin models was assessed and optimized using iterative cycles of real-space refinement with the program PHENIX and manual rebuilding with Coot to diminish Ramachandran outliers, atom clashes, and to optimize rotamer positions to the central EM density (See Figs. S1 and S2; Table S2; (33,34)).

Protein-protein docking

The position of tropomyosin on S1 decorated F-actin was characterized through a global conformational search, using the programs PIPER and ClusPro (16,17) as previously implemented for S1-free F-actin and described in detail (18). In brief, the search was conducted using a series of tropomyosin segments as ligands and acto-S1 as the receptor. Indeed, tropomyosin is a modular protein, which in the muscle isoform consists of seven pseudorepeating elements each represented by tandem α-zones and β-zones; in thin filaments, α-zones lie over subdomains 1 and 3 of actin, and β-zones lie over subdomains 2 and 4 of actin. Each tropomyosin segment here contained of two consecutive α-zones of tropomyosin with an intervening β-zone (58 amino acids in total and ~85 Å in length). These were docked to atomic model targets comprised of two actin monomers both linked to an S1, using our cryo-EM reconstruction model, where the end of S1 distal to actin was truncated (residues 35–217 and 625–776 were removed) to focus the computation search on the acto-S1 interface. Tropomyosin fragments used for docking were defined as $\alpha_1\beta_1\alpha_2$ (residues 8–66), $\alpha_2\beta_2\alpha_3$ (residues 47–105), $\alpha_3\beta_3\alpha_4$ (residues 86–145), $\alpha_4\beta_4\alpha_5$ (residues 127–184), $\alpha_5\beta_5\alpha_6$ (residues 165–223), $\alpha_6\beta_6\alpha_7$ (residues 205–263) segments, and N- and C-terminal overlapping domains consisting of $\alpha_1\beta_1\alpha_2$ (residues 1–66) and $\beta_6\alpha_7\beta_7$ (residues 230–284). The top ranked structures for each of the segments in the docking trials (Fig. 2, *A–F*) were ascertained based on a combination of van der Waals and electrostatic criteria and they were judged further by visual inspection of protein-protein interactions, polarity relative to the F-actin axis and superimposition onto the above cryo-EM reconstruction with the use of UCSF Chimera (27).

Construction and refinement of tropomyosin models

Once tropomyosin docking was completed, the fragments were assembled computationally into a pseudoatomic model by splicing them together to form a continuous tropomyosin model on acto-S1 (Fig. 2 *G*). The first common α-zone between any two respective fragments were superimposed, and then continuing in this manner an entire chain was created. The resulting models were then subjected to flexible fitting refinement to the cryo-EM volume reference structure (MDFF) (31) and by standard molecular dynamics in explicit solvent (Fig. 3, *A* and *B*).

To address the tropomyosin head-to-tail overlapping domain interaction with S1, a model of full-length tropomyosin on fully decorated acto-S1 was built starting from an ideal superhelical coiled coil structure (35) that had been optimized by MDFF flexible fitting to the EM density map. A docked overlap domain and surrounding residues were then threaded into the mid-piece of the tropomyosin model by combining common residues and the entire structure energy minimized, as done previously (18). The resulting actin-S1-tropomyosin construct was extended to a cable model in a periodic boundary system (18) to simulate tropomyosin dynamics on an infinite long filament during molecular dynamics. Molecular dynamics was carried out using explicit solvent, as previously (18,32) for 30 ns.

RESULTS AND DISCUSSION

The following sections detail and appraise results of our stepwise approach in building an atomic model of S1-decorated actin-tropomyosin filaments and in determining the cardiac muscle myosin-head-tropomyosin interaction.

The reconstruction

To evaluate how the binding of myosin affects tropomyosin position, actin-tropomyosin filaments were saturated with myosin-S1 in the absence of ATP, thus reflecting myosin on actin in the "rigor" configuration. Our cryo-EM 3D reconstruction of the S1-decorated filament achieved a

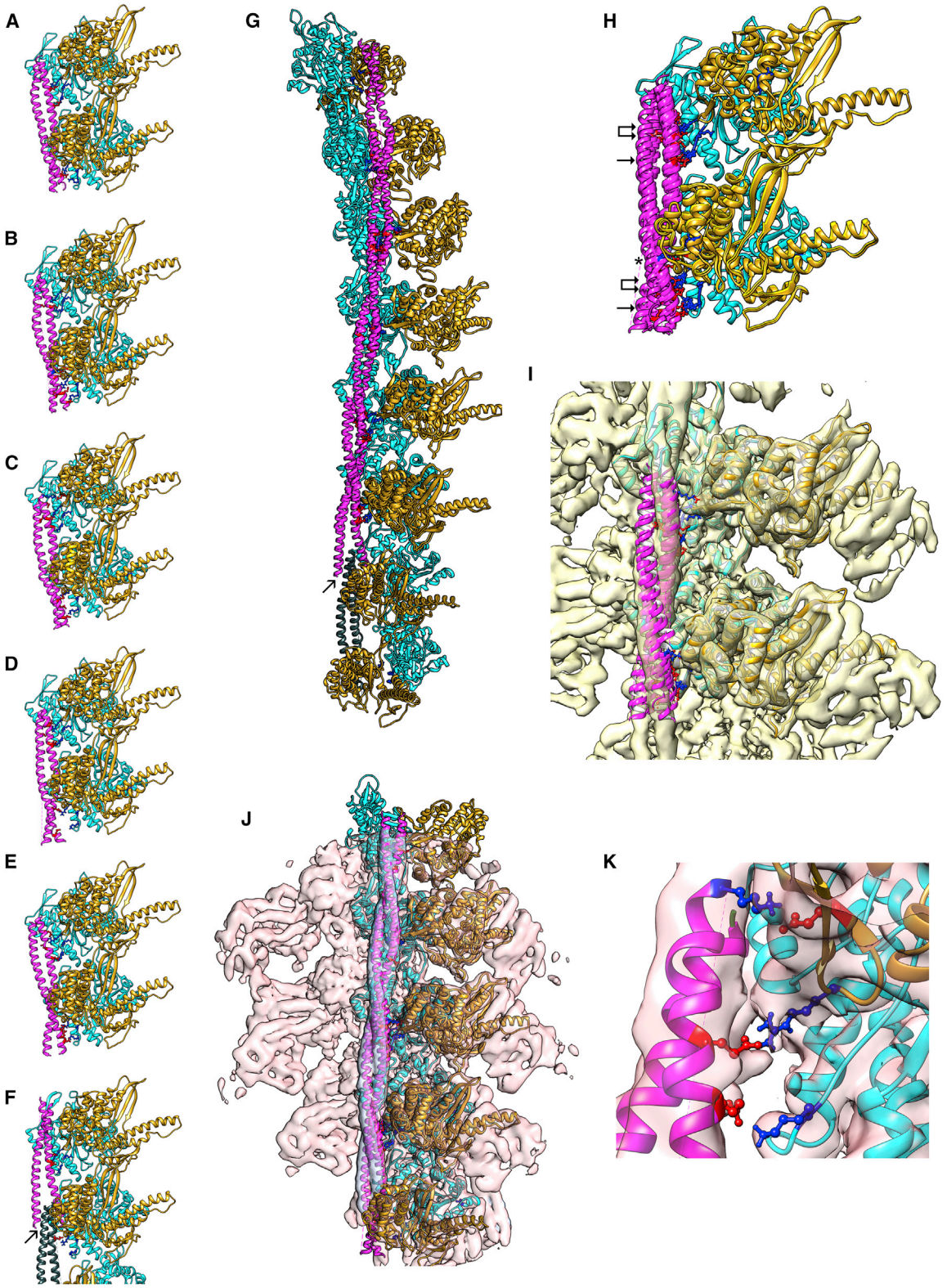

FIGURE 2 Docking tropomyosin segments to S1-decorated F-actin. (*A–F*) Highest scoring $\alpha\beta\alpha$-zone tropomyosin segments docked to acto-S1 (tropomyosin, *magenta*; S1, *gold*; actin, *cyan*), showing tropomyosin poses on acto-S1 associated with fragment (*A*) $\alpha_2\beta_2\alpha_3$, (*B*) $\alpha_3\beta_3\alpha_4$, (*C*) $\alpha_4\beta_4\alpha_5$, (*D*) $\alpha_5\beta_5\alpha_6$, (*E*) $\alpha_6\beta_6\alpha_7$, and (*F*) the overlapping domain (*arrow*) and surrounding residues, i.e., $\beta_6\alpha_7\beta_7\alpha_1\beta_1\alpha_2$. Ribbon diagrams are shown with sidechains on actin Lys326 and Lys328 as well as on myosin Arg369 colored blue, along with their interacting partners on tropomyosin in the M-state, colored red. In (*A*)–(*F*), segments are offset by one actin subunit and thus, each is related to the next by one common subunit. In (*G*), the common parts of segments shown in (*A*)–(*F*) were

(legend continued on next page)

resolution of 4.2 Å and shows that myosin-S1 makes extensive contact with the actin subdomains 1 and 2 on the outer aspect of actin subunits (Fig. 1; Table S3). Conversely, tropomyosin lies entirely over the actin subdomains 3 and 4 on the inner aspect of actin. These results are common to all previous reconstructions of M-state thin filaments dating back 30 years (8–12,36). Despite an ∼13° average rotational translation of tropomyosin around the actin filament and very small longitudinal shift (0.6 Å) over actin to the M-state from the previously delineated C-state position (12,18), the current reconstruction shows relatively little direct contact between myosin and tropomyosin except for a well-resolved extra density emerging from the tip of myosin head. This density, representing loop 4 of myosin, bridges the border between actin subdomains 1 and 3 and extends to the tropomyosin density (Fig. 1, *red arrows* in Fig. 1 *A* mark the loop 4 projection, which is most easily viewed by zooming-in to an ∼2-fold magnification).

Fitting actin and S1 to the reconstruction

As mentioned, the well-defined secondary structure as well as side chain density captured by the thin filament reconstruction allows high-resolution structural models to be fitted accurately into corresponding cryo-EM density map. Skeletal muscle F-actin (e.g., PDB: 6KN8) fitted directly to corresponding densities in the reconstruction map without noticeable changes to the structure during follow-up flexible fitting (Fig. 1). Individual actin densities in common with side-chain functional groups in the atomic model were visible in most of the actin structure. The actin subunit configuration in the maps (Electron Microscopy Data Bank ID: EMD-22067; PDB: 6X5Z) are completely consistent with prior solutions irrespective of the actin source (10–12,14,16).

High-resolution structures of vertebrate muscle myosin-S1 in a nucleotide-free "rigor state" have not been solved and therefore are not available to merge into the cryo-EM map nor to characterize the S1 conformation. After the procedure of Fujii and Namba (12) (see Materials and Methods for details and rationale), a homology model of S1 was therefore built based on a crystal structure of squid muscle S1 in its rigor-like state (PDB: 3I5G, from fast funnel retractor muscle). The model was then fitted into its corresponding density volume in the reconstruction and its complementarity to the map refined by flexible fitting to match residue-level density and further using the programs PHENIX and Coot (33,34). A composite atomic model, containing both fitted actin and S1, shows residue-to-residue contacts at the interface between actin and S1, which are the same as previously proposed (10–12); namely S1 interacts extensively with the actin surface via the so-called cardiomyopathy loop (residues Thr417 to Pro402), loop 4 (residues Gly360 to Glu379), and the helix-loop-helix motif (residues Ile530 to His556) (Fig. 1; Table S3; Electron Microscopy Data Bank ID: EMD-22067; PDB: 6X5Z; the sequence coding Q9BE39 for MYH7_BOVIN is cited). Our main interest here, however, concerns residue-to-residue interactions between tropomyosin and acto-S1, which as outlined above have remained ambiguous.

The two chains of the tropomyosin coiled coil are easily visible in our reconstruction. The average 137 Å helical pitch of the coiled coil around its own axis is well-characterized and retained in the cryo-EM map. However, because of helical averaging, the short 9–11 residue overlapping domain itself is lost during image processing. In addition, the localized over- and undertwisting of residues in tropomyosin pseudorepeats 1 and 7 (18,37) required during the overlapping domain assembly also are not retained, but can be assessed computationally (see below).

Myosin loop 4 approaches tropomyosin closely

A focus was placed on possible interactions of loop 4 of myosin which interacts closely with tropomyosin. As noted above, in addition to contacting the surface of actin, the loop 4 density protrusion extends from the end of myosin's upper 50K domain in the direction of tropomyosin. Here, loop 4 reaches over the border between subdomain 1 and 3 of actin and toward the underside of the tropomyosin coiled coil lying on actin (Fig. 1 *C*). Not only is the loop 4 density well-resolved in the reconstruction, but the homology model fitting identifies the individual residues comprising loop 4 and the adjoining tropomyosin. Moreover, conspicuous extra density is observed to project outward at the very tip of the protruding amino acid loop that represents the side chain of arginine 369 pointing toward tropomyosin. As discussed below, Arg369 of the myosin head may act to

superposed to generate a composite "single-stranded" actin-tropomyosin filament; the arrow points to residues in the overlapping domain that form a four-helix bundle in (*F*). In (*H*), segments (*A*)–(*E*) were directly superposed on each other. Note the superposed motif of actin Lys326 (*blue*, *single arrows*) and of myosin Arg369 (*blue*, *double arrows*) interacting with sidechains of oppositely charged residues on the various tropomyosin fragments (*red*); also note occasional interaction of myosin Glu374 and tropomyosin (*asterisk*). (*I*) superposed segments fitted within the isosurface of the reconstruction in Fig. 1, using the "Fit in Map" program in UCSF Chimera (27), and similarly in (*J*), segments $\alpha_2\beta_2\alpha_3$, $\alpha_3\beta_3\alpha_4$, $\alpha_4\beta_4\alpha_5$, and $\alpha_5\beta_5\alpha_6$ from the pseudoatomic map in (*G*) were fitted to the reconstruction. (*K*) Enlargement of tropomyosin pseudorepeat 4 region in (*J*), showing side-chain interactions between actin Lys326 and tropomyosin Glu142 (*bottom pair*), myosin Arg369 and tropomyosin Glu138 (*middle pair*), and myosin Glu374 and tropomyosin Lys128 (*top pair*). Please note that the docking in (*A*)–(*F*), as well as the superimposition of segments in (*G*)–(*J*) and "Fit in Map" alignment to cryo-EM reconstructions in (*I*) and (*K*), did not involve any flexible fitting routines or other manipulation of respective coordinates, i.e., only "raw" PIPER/ClusPro output was evaluated. S1 residues 217–623 are shown in the ribbon models displayed because, here, the end of S1 distal to actin was truncated (residues 35–216 and 624–776 were removed) to focus the computation search on the acto-S1 interface. Pointed end of actin was facing up in all panels. To see this figure in color, go online.

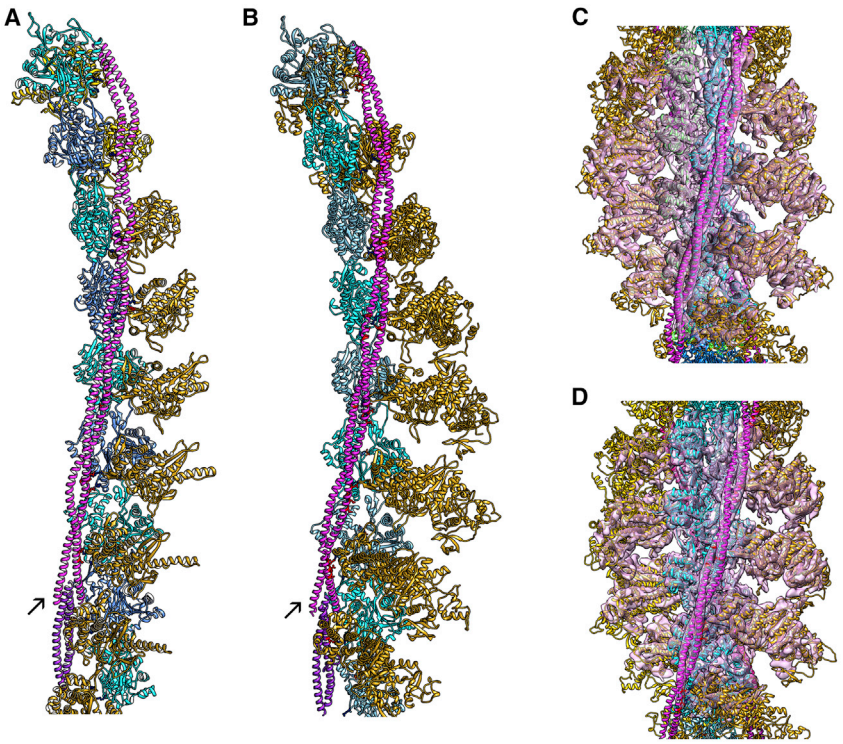

FIGURE 3 Annealing docked segments together and molecular dynamics of the M-state model. This figure has the same color coding as in Figs. 1 and 2; in (*A*) and (*B*) only a single-helical strand of F-actin and associated proteins are shown. (*A*) Respective tropomyosin pseudorepeats docked to actin-S1 segments in Fig. 2, A–F shown annealed together by flexible fitting routines. (*B*) An atomic model of M-state filaments subjected to molecular dynamics in explicit solvent. The MD was started from a canonical model of tropomyosin fitted to the cryo-EM 3D-reconstruction and then threaded into the structure of the tropomyosin overlapping domain complex, i.e., structures described in (15) and (18). The tropomyosin-coiled coil remained intact and its position on actin stable throughout simulation; side-chain interactions from tropomyosin to actin and S1 are noted on Table 1 and highlighted in the figure (*red* and *blue* for respective acidic and basic residues). The representative trajectory snapshot shown in (*B*) was taken from the 30-ns time period of simulation and is a frame that had minimal root mean-square deviation from the average structure over that time period (calculated by backbone atoms superimposition). In (*C*) and (*D*), the respective midpieces of the modeled filaments (representing repeats 2–6) shown in (*A*) and (*B*) were fitted within densities of the reconstruction of S1-decorated acto-tropomyosin. Note that the construction of starting models in (*A*) and (*C*) and in (*B*) and (*D*) differed yet yielded virtually the same outcomes. Arrows indicate the position of the tropomyosin overlapping domain in (*A*) and (*B*). In (*A*), S1 residues 217–623 are shown in ribbon format, and in (*B*)–(*D*), the full S1 ribbon structure (to residue 777) is shown. To see this figure in color, go online.

reposition tropomyosin from its default C-state position on actin and stabilize it in the M-state location. In the process, C-state tropomyosin interactions with actin residues Lys326 and Lys328 (18) appear to be replaced by ones on myosin Arg369 and more fleeting new links to Lys326.

Molecular level docking of tropomyosin segments to S1-decorated actin

To date, individual tropomyosin residues have not been resolved in cryo-EM maps (8–15,36), leaving modeling of thin filament regulatory mechanisms uncertain. A bottom-up computational approach was therefore taken here to perform M-state tropomyosin docking onto the S1-decorated actin to determine potential residue-to-residue contacts formed between tropomyosin and myosin. Cardiac tropomyosin ($\alpha\alpha$-Tpm1.1) was first divided computationally into a series of overlapping segments centered on successive tropomyosin β-zones within individual tropomyosin pseudorepeats. Each β-zone was flanked on both its ends by respective α-zones, thus yielding a series of $\alpha_i\beta_i\alpha_{i+1}$ fragments. We previously found this segment length was the shortest needed for PIPER/ClusPro programs to dock segments of the coiled coil protein onto F-actin with known superhelical orientation and polarity (18). In the current study, the same tropomyosin fragments were docked to the S1-decorated F-actin structure determined above. The docking required a minimum size acto-S1 "receptor" containing two longitudinally linked actin subunits, each associated with S1 motors in a nucleotide-free "rigor" conformation. This arrangement yielded tropomyosin poses with correct superhelical orientation and polarity (Fig. 2, *A–G*). After docking, all $\alpha_i\beta_i\alpha_{i+1}$ segments examined (i.e., $\alpha_2\beta_2\alpha_3$, $\alpha_3\beta_3\alpha_4$, $\alpha_4\beta_4\alpha_5$, $\alpha_5\beta_5\alpha_6$, $\alpha_6\beta_6\alpha_7$) produced tropomyosin α-zone structural motifs facing acto-S1, and with individual α-zones in common or entire segments being superposable (Fig. 2, *H* and *I*). In all instances, acidic residues on one or both chains of tropomyosin come within 5 Å of the oppositely charged terminal guanidino side chain of Arg369 which extend from myosin loop 4 (Table 1). In fact, Arg369 of loop 4 is buttressed on one side by Gln368 and Arg367, conserved in all mammalian sarcomeric myosin II isoforms, presumably to maintain a positively charged local environment that strengthens tropomyosin contacts (see Table S1). In addition, neighboring acidic residues on tropomyosin (e.g., residues 104, 142, 180) contact Lys326 on successive actin subunits. These contacts appear to form a second set of interactions with tropomyosin (Fig. 2). Thus, it is attractive to consider that myosin-S1 relocates tropomyosin away from its C-state interactions with actin (18), while creating new contacts with actin and tropomyosin. In the process, tropomyosin moves azimuthally ~13° (9 Å) from its C-state position and less than 1 Å in its longitudinal placement.

Because each tropomyosin fragment docked to acto-S1 was offset from the next by approximately one-half pseudorepeat,

TABLE 1 Charged Residues that Closely Contact Each Other in the M-State; Tropomyosin and Arginine 369 on Myosin Loop 4; Tropomyosin and Lysine 326 on Actin

		ClusPro Docking		MD	
		Myosin Arg369	Actin Lys326	Myosin Arg369	Actin Lys326
Actin Subunit	Tpm Period	Tropomyosin Residue		Tropomyosin Residue	
7	1	Glu16*	–	Glu16*	Asp20*, Glu23*
6	2	Glu58	Glu69	Glu54*, Asp58*	Glu69
5	3	Glu97, Glu98	Glu104*	Glu96*, Glu104	Glu100*, Glu104*
4	4	Asp137, Glu138*	Glu142*	Glu131*, Asp137*, Glu138*	Glu142*
3	5	Glu173*, Asp175	Glu180*, Glu181	Glu173, Asp175*, Glu180*	Glu180*, Glu181
2	6	Glu212, Glu218	Asp219, Glu223*	Glu212, Glu218*	Asp219, Glu223
1	7	Asp254, Glu257*	Asp258	Glu250*, Asp254*, Glu257*	Asp258

Residue-to-residue contacts determined for structures displayed in Fig. 3. Acidic residues on tropomyosin within 10 Å of basic ones either on myosin or on actin are listed. Residues underlined in the third and fourth columns were determined by ClusPro docking (a static measurement) to lie less than 5 Å from their oppositely charged partners and those additionally flagged by an asterisk were separated by less than 2 Å. Residues underlined in the fifth and sixth columns were determined by MD (which measures dynamic interactions) to lie "on average" less than 5 Å of oppositely charged partners and those making intermittent contacts with each other by less than 2 Å are marked by asterisks. The docking studies also showed contact made between Glu374 on myosin and Lys128 on tropomyosin (<5 Å apart); during MD, contacts are often noted between Glu374 on myosin and residues Lys12, Lys128, and Lys205 on tropomyosin (<2 Å apart).

their sequences in common could also be superposed together (e.g., $\alpha_2\beta_2\alpha_3 + \alpha_3\beta_3\alpha_4$ to yield $\alpha_2\beta_2\alpha_3\beta_3\alpha_4$; $\alpha_2\beta_2\alpha_3\beta_3\alpha_4 + \alpha_4\beta_4\alpha_5$ to yield $\alpha_2\beta_2\alpha_3\beta_3\alpha_4\beta_4\alpha_5$, etc.). In this way, tropomyosin with its underlying actin and S1 substructure formed a complete pseudoatomic model of an S1-decorated filament (Fig. 2 *G*). Even though all segment-associated tropomyosin fragments fitted within densities in the cryo-EM reconstruction, periods 2, 3, 4, and 5 of tropomyosin (derived from $\alpha_2\beta_2\alpha_3$, $\alpha_3\beta_3\alpha_4$, and $\alpha_4\beta_4\alpha_5$) aligned best to the EM volume (Fig. 2, *I–K*). To more faithfully display tropomyosin strand continuity, these actin-tropomyosin-S1 segments were flexibly fitted to the cryo-EM map, which allowed their ends to anneal to form seamless cables on F-actin (Fig. 3, *A* and *C*). This was achieved without constraining the respective axial or azimuthal positioning of the tropomyosin. The refined tropomyosin cables were then subjected to MD simulation, maintaining all the same residue-to-residue contacts with actin noted above (Fig. 3, *B* and *D*). Thus, the results of the docking and the cryo-EM procedures cross-validate each other.

Thus, the PIPER/ClusPro-derived model of actin, tropomyosin, and S1 fitted well within the EM densities with accuracy already noted for atomic structure fitting shown in Fig. 1. Not only are Asp369 residues on S1 loop 4 particularly well fitted, but the side chains of actin residue Lys326 are also oriented toward oppositely charged tropomyosin targets (Figs. 2, *J* and *K* and 3 *C*) on each pseudorepeat. As noted above, the latter residue is strongly associated with actin-tropomyosin binding in different regulatory states.

Docking the tropomyosin overlapping domain to S1-decorated actin and MD on the full acto-tropomyosin-S1 complex

The tropomyosin overlapping domain docks precisely to S1-decorated actin without clashing with S1 residues and thus does not obstruct the myosin-binding site on actin (Fig. 2 *F*). Notably, the additional local presence of TnT1, modeled as in (18), also does not obstruct myosin-binding (data not shown). Indeed, PIPER/ClusPro docking indicates that repeats 2–6 as well as the overlapping domain appear to undergo a strict azimuthal sliding from their C-state to their M-state position without obvious conformational reconfiguration or significant longitudinal translation. A preliminary model of full-length tropomyosin in the M-state configuration was therefore constructed computationally by threading pseudorepeats 2–6 to the overlapping domain. MD was carried out, and the composite model remained stable over time. However, loop 4 was seen to be flexible, possibly to optimize Arg369 orientation to favorably target residues on tropomyosin, thus compensating for mismatched thick and thin filament symmetry in vertebrate muscle. Loop 4 flexibility may also contribute to Arg369 promiscuity observed during MD, allowing it the freedom to interact with one or another closely neighboring acidic residues on tropomyosin. Thus, the apparent flexibility of loop 4 may provide a mechanism for myosin heads to adjust to the slight mismatches in orientation and optimize contact of tropomyosin during the cross-bridge cycle on thin filaments. Glu374 on loop 4 also interacts transiently with basic residues on tropomyosin as does Lys326 on actin with acidic residues on tropomyosin, thus bolstering interactions.

Tropomyosin's roadmap from C to shining M

Cryo-EM reconstruction and tropomyosin docking protocols have identified structures that offer a glimpse of average end-state regulatory structures that reflect blocked, closed, and open biochemical states (see Fig. S3; (8–15)). In turn, these structures provide insights about the roadmap that myosin must navigate while transitioning between thin filament activation and relaxation. Simply overlaying the M-state S1 configuration over B- or C-state actin-tropomyosin (8–15) shows that loop 4 of myosin clashes with tropomyosin in pre-power stroke myosin-head configurations (for example, see

(9–11)). This steric clash is expected to prevent cleft closure between the upper and lower 50K domains of the myosin head, which is required for strong myosin-actin interaction and productive cross-bridge cycling to occur on actin filaments during muscle contraction (8–11). Thus, steric interference by tropomyosin in both the low Ca^{2+}-linked blocked B-state and the high Ca^{2+}-linked C-state will inhibit myosin interaction with actin and therefore contraction (8,9). Without tropomyosin displacement from both B- and C-state positions, muscles cannot contract. At low-Ca^{2+}, TnI constrains tropomyosin sufficiently that myosin.ADP.P_i cannot nudge tropomyosin strongly enough to overcome the steric interference imposed by the B-state thin filament (15). It is also possible that localized charge repulsion between loop 4 and TnI-stabilized tropomyosin may further limit the possibility of actin-myosin interaction. However, once tropomyosin is freed of TnI-imposed constraints at high Ca^{2+}, any charge repulsion between loop 4 of weakly bound myosin in the C-state may now promote tropomyosin movement toward the M-state as alluded to by Vibert et al. (8). Alternatively, tropomyosin simply may be propelled toward the M-position by myosin's competition for residues on actin around the C-state binding site for tropomyosin, effectively pushing tropomyosin away. These alternatives are difficult to decipher energetically or at present by cryo-EM. Equally uncertain is the temporal order of myosin cleft closure, the myosin power stroke, P_i release from myosin after ATP hydrolysis and M-state myosin binding itself or, indeed, if there is a true fixed order. Clearly, weak binding of myosin to C-state thin filaments occurs (2), but when in a kinetic scheme, myosin cleft closure happens has not as yet been revealed by cryo-EM.

In any event, the first myosin bound to C-state actin is expected to have an ~80% chance of nudging tropomyosin to the M-state position (2,38), accompanied by cleft closure between the myosin upper and lower 50K domains. Then, in a coordinated way, tropomyosin movement from C- to M-states drops myosin loop 4 to a site directly opposed to tropomyosin, likely trapping tropomyosin in the M-state (11), which is coupled to a new local electrostatic energy valley. Little or no additional nudging would be needed to sustain the M-state and promote additional myosin-binding events, given the high persistence length of tropomyosin (39). It is noteworthy that our studies support the premise that myosin-tropomyosin interaction is involved in thin filament regulatory transitions (5–7).

It is often noted that tropomyosin function is strongly coupled to its unique coiled-coil-structural patterning (40), and this leitmotif is a recurring theme of the current and previous articles (18,37,40,41). It is also worth emphasizing that experimental deletion of the central repeat period regions 3, 4, and 5 greatly reduces tropomyosin affinity for myosin-bound actin filaments but has little effect on tropomyosin interaction with myosin-free thin filaments, suggesting that binding between tropomyosin and myosin on actin is pseudodomain specific (42–44). Interestingly, our structural work indicates that although all pseudorepeats of tropomyosin contain specific acidic residues likely to interact with myosin loop 4 during the M-state, the central group of tropomyosin pseudorepeats contain relatively larger clusters of acidic residues poised to link to Arg369 on loop 4. Thus, the midpiece of tropomyosin could represent a particularly favorable target for the myosin-head-binding actin, leaving pseudorepeats 1 and 7 with a more restricted role, namely forming the tropomyosin-overlapping domain and, therefore, having lower probability of myosin binding. It is also worth noting that noncanonical *d*-position tropomyosin residue Asp137 in pseudorepeat 4, which is strictly conserved phylogenetically, may be required to prime the midpiece of the tropomyosin-coiled coil as a hot spot for myosin-binding. The absence of stabilizing electrostatic linkages formed by residues Glu131 and Glu138 between tropomyosin's coiled coil α-helices (i.e., *e-g* pairing) is also notable (depicted in Fig. 1 of (41)), possibly serving the same purpose. The functional importance of tropomyosin pseudorepeat 4 is additionally underscored by the observation that few, if any, mutation-linked cardiomyopathies are attributed to this sequence. This suggests that such perturbations might not be compatible with life. These and other possibilities are well-suited for further investigation.

SUPPORTING MATERIAL

Supporting Material can be found online at https://doi.org/10.1016/j.bpj.2020.07.006.

AUTHOR CONTRIBUTIONS

W.L. thought of the general approach taken and along with M.H.D., M.J.R., E.P., J.R.M., M.R., and M.A.G. formulated the principal concepts presented. M.H.D. performed the cryo-EM, generated the 3D reconstruction, and did the hybrid crystallography; he was trained and advised jointly by W.L., E.B., and M.J.R. E.P. carried out the docking studies. E.P. and M.J.R. performed the molecular dynamics simulations. J.W. prepared the masseter S1 and carried out the myosin sequence analyses. All authors participated in data analysis and interpretation. W.L. and M.H.D. wrote the manuscript. M.H.D., W.L., and J.W. prepared the figures and tables.

ACKNOWLEDGMENTS

This work was funded by National Institutes of Health (NIH) Grants R01HL036153 (to W.L.), R01HL123774 (to J.R.M. and W.L.), P30AR074990, RM1GM131981, R01HL128368 (to M.R.), and R01GM029090 (awarded to Leslie A. Leinwand and sponsoring M.A.G.). M.A.G., J.W., and M.R. were also supported by the European Union's Horizon 2020 Research and Innovation Programme Grant 777204 SILICOFCM. M.H.D. was supported by NIH Training Program Grant T32HL007969 (to Katya Ravid) and by the Boston University Division of Graduate Medical Sciences institutional funds. Computational work was carried out in house and using resources provided by the Massachusetts Green High Performance Computing Center. Preliminary screening of electron microscope samples was carried out in house and supported by NIH Grant S10RR25434 (to E.B.); the rest of the electron microscope work was performed at the Stanford Linear Accelerator Center Cryo-EM Facilities (S2C2) supported by Stanford University and the NIH Common Fund Transformative High-Resolution Cryoelectron Microscopy Program

(U24 GM129541) as well as NIH Grant U24GM116787 (to Wah Chiu). Some of this work was performed at the Regional Cryo-EM Consortium, which is also supported by NIH funding (U24GM116787) and the S10 Instrumentation Programs (S10OD021600). The content of the work presented is solely the responsibility of the authors and does not represent the official views of the NIH or the European Union.

REFERENCES

1. Gordon, A. M., E. Homsher, and M. Regnier. 2000. Regulation of contraction in striated muscle. *Physiol. Rev.* 80:853–924.
2. Geeves, M. A. 2012. Thin filament regulation. *In* Comprehensive Biophysics: Molecular Motors and Motility, *Volume 4*. E. H. Egelman, Y. E. Goldman, and E. M. Ostap, eds.. Academic Press, pp. 251–267.
3. Lehman, W. 2016. Thin filament structure and the steric blocking model. *Compr. Physiol.* 6:1043–1069.
4. Holmes, K. C., and W. Lehman. 2008. Gestalt-binding of tropomyosin to actin filaments. *J. Muscle Res. Cell Motil.* 29:213–219.
5. Lehrer, S. S. 1994. The regulatory switch of the muscle thin filament: Ca^{2+} or myosin heads? *J. Muscle Res. Cell Motil.* 15:232–236.
6. Golitsina, N. L., and S. S. Lehrer. 1999. Smooth muscle α-tropomyosin crosslinks to caldesmon, to actin and to myosin subfragment 1 on the muscle thin filament. *FEBS Lett.* 463:146–150.
7. Lehrer, S. S. 2011. The 3-state model of muscle regulation revisited: is a fourth state involved? *J. Muscle Res. Cell Motil.* 32:203–208.
8. Vibert, P., R. Craig, and W. Lehman. 1997. Steric-model for activation of muscle thin filaments. *J. Mol. Biol.* 266:8–14.
9. Poole, K. J., M. Lorenz, …, K. C. Holmes. 2006. A comparison of muscle thin filament models obtained from electron microscopy reconstructions and low-angle X-ray fibre diagrams from non-overlap muscle. *J. Struct. Biol.* 155:273–284.
10. Behrmann, E., M. Müller, …, S. Raunser. 2012. Structure of the rigor actin-tropomyosin-myosin complex. *Cell.* 150:327–338.
11. von der Ecken, J., S. M. Heissler, …, S. Raunser. 2016. Cryo-EM structure of a human cytoplasmic actomyosin complex at near-atomic resolution. *Nature.* 534:724–728.
12. Fujii, T., and K. Namba. 2017. Structure of actomyosin rigour complex at 5.2 Å resolution and insights into the ATPase cycle mechanism. *Nat. Commun.* 8:13969.
13. Lehman, W., M. Orzechowski, …, S. Raunser. 2013. Gestalt-binding of tropomyosin on actin during thin filament activation. *J. Muscle Res. Cell Motil.* 34:155–163.
14. von der Ecken, J., M. Müller, …, S. Raunser. 2015. Structure of the F-actin-tropomyosin complex. *Nature.* 519:114–117.
15. Yamada, Y., K. Namba, and T. Fujii. 2020. Cardiac muscle thin filament structures reveal calcium regulatory mechanism. *Nat. Commun.* 11:153.
16. Kozakov, D., D. R. Hall, …, S. Vajda. 2010. Achieving reliability and high accuracy in automated protein docking: ClusPro, PIPER, SDU, and stability analysis in CAPRI rounds 13-19. *Proteins.* 78:3124–3130.
17. Kozakov, D., D. R. Hall, …, S. Vajda. 2017. The ClusPro web server for protein-protein docking. *Nat. Protoc.* 12:255–278.
18. Pavadai, E., W. Lehman, and M. J. Rynkiewicz. 2020. Protein-protein docking reveals dynamic interactions of tropomyosin on actin filaments. *Biophys. J.* 119:75–86.
19. Bloemink, M. J., N. Adamek, …, M. A. Geeves. 2007. Kinetic analysis of the slow skeletal myosin MHC-1 isoform from bovine masseter muscle. *J. Mol. Biol.* 373:1184–1197.
20. Coulton, A. T., K. Koka, …, M. A. Geeves. 2008. Role of the head-to-tail overlap region in smooth and skeletal muscle beta-tropomyosin. *Biochemistry.* 47:388–397.
21. Spudich, J. A., and S. Watt. 1971. The regulation of rabbit skeletal muscle contraction. I. Biochemical studies of the interaction of the tropomyosin-troponin complex with actin and the proteolytic fragments of myosin. *J. Biol. Chem.* 246:4866–4871.
22. Noble, A. J., H. Wei, …, B. Carragher. 2018. Reducing effects of particle adsorption to the air-water interface in cryo-EM. *Nat. Methods.* 15:793–795.
23. Scheres, S. H. 2012. RELION: implementation of a Bayesian approach to cryo-EM structure determination. *J. Struct. Biol.* 180:519–530.
24. Scheres, S. H. 2016. Processing of structurally heterogeneous cryo-EM data in RELION. *Methods Enzymol.* 579:125–157.
25. He, S., and S. H. W. Scheres. 2017. Helical reconstruction in RELION. *J. Struct. Biol.* 198:163–176.
26. Tang, G., L. Peng, …, S. J. Ludtke. 2007. EMAN2: an extensible image processing suite for electron microscopy. *J. Struct. Biol.* 157:38–46.
27. Pettersen, E. F., T. D. Goddard, …, T. E. Ferrin. 2004. UCSF Chimera–a visualization system for exploratory research and analysis. *J. Comput. Chem.* 25:1605–1612.
28. Yang, Y., S. Gourinath, …, C. Cohen. 2007. Rigor-like structures from muscle myosins reveal key mechanical elements in the transduction pathways of this allosteric motor. *Structure.* 15:553–564.
29. Waterhouse, A., M. Bertoni, …, T. Schwede. 2018. SWISS-MODEL: homology modelling of protein structures and complexes. *Nucleic Acids Res.* 46:W296–W303.
30. Robert-Paganin, J., D. Auguin, and A. Houdusse. 2018. Hypertrophic cardiomyopathy disease results from disparate impairments of cardiac myosin function and auto-inhibition. *Nat. Commun.* 9:4019.
31. Trabuco, L. G., E. Villa, …, K. Schulten. 2009. Molecular dynamics flexible fitting: a practical guide to combine cryo-electron microscopy and X-ray crystallography. *Methods.* 49:174–180.
32. Phillips, J. C., R. Braun, …, K. Schulten. 2005. Scalable molecular dynamics with NAMD. *J. Comput. Chem.* 26:1781–1802.
33. Afonine, P. V., B. K. Poon, …, P. D. Adams. 2018. Real-space refinement in PHENIX for cryo-EM and crystallography. *Acta Crystallogr. D Struct. Biol.* 74:531–544.
34. Emsley, P., B. Lohkamp, …, K. Cowtan. 2010. Features and development of Coot. *Acta Crystallogr. D Biol. Crystallogr.* 66:486–501.
35. Lorenz, M., K. J. Poole, …, K. C. Holmes. 1995. An atomic model of the unregulated thin filament obtained by X-ray fiber diffraction on oriented actin-tropomyosin gels. *J. Mol. Biol.* 246:108–119.
36. Milligan, R. A., M. Whittaker, and D. Safer. 1990. Molecular structure of F-actin and location of surface binding sites. *Nature.* 348:217–221.
37. Lehman, W., M. J. Rynkiewicz, and J. R. Moore. 2020. A new twist on tropomyosin binding to actin filaments: perspectives on thin filament function, assembly and biomechanics. *J. Muscle Res. Cell Motil.* 41:23–38.
38. McKillop, D. F., and M. A. Geeves. 1993. Regulation of the interaction between actin and myosin subfragment 1: evidence for three states of the thin filament. *Biophys. J.* 65:693–701.
39. Li, X. E., K. C. Holmes, …, S. Fischer. 2010. The shape and flexibility of tropomyosin coiled coils: implications for actin filament assembly and regulation. *J. Mol. Biol.* 395:327–339.
40. Hitchcock-DeGregori, S. E. 2008. Tropomyosin: function follows structure. *Adv. Exp. Med. Biol.* 644:60–72.
41. Lehman, W., X. Li, …, M. J. Rynkiewicz. 2018. Precise binding of tropomyosin on actin involves sequence-dependent variance in coiled-coil twisting. *Biophys. J.* 115:1082–1092.
42. Hitchcock-DeGregori, S. E., and B. Barua. 2017. Tropomyosin structure, function, and interactions: a dynamic regulator. *Subcell. Biochem.* 82:253–284.
43. Landis, C., N. Back, …, L. S. Tobacman. 1999. Effects of tropomyosin internal deletions on thin filament function. *J. Biol. Chem.* 274:31279–31285.
44. Hitchcock-DeGregori, S. E., Y. Song, and J. Moraczewska. 2001. Importance of internal regions and the overall length of tropomyosin for actin binding and regulatory function. *Biochemistry.* 40:2104–2112.

Biophysical Journal, Volume *119*

Supplemental Information

Cryo-EM and Molecular Docking Shows Myosin Loop 4 Contacts Actin and Tropomyosin on Thin Filaments

Matthew H. Doran, Elumalai Pavadai, Michael J. Rynkiewicz, Jonathan Walklate, Esther Bullitt, Jeffrey R. Moore, Michael Regnier, Michael A. Geeves, and William Lehman

Species/myosin isoform	Residues																								
Sarcomeric myosins 2	**359**	**360**	**361**	**362**	**363**	**364**	**365**	**366**	**367**	**368**	**369**	**370**	**371**	**372**	**373**	**374**		**375**	**376**	**377**	**378**	**379**	**380**	**381**	**382**
Bovine MyHC-β – slow skeletal, cardiac	F	G	N	M	K	F	K	L	K	Q	R	E	E	Q	A	E	-	P	D	G	T	E	E	A	D
Human MyHC-β – slow skeletal, cardiac	F	G	N	M	K	F	K	Q	K	Q	R	E	E	Q	A	E	-	P	D	G	T	E	E	A	D
Human MyHC-2x fast skeletal	Y	G	N	M	K	F	K	Q	K	Q	R	E	E	Q	A	E	-	P	D	G	T	E	V	A	D
Human MyHC-2a fast skeletal	Y	G	N	L	K	F	K	Q	K	Q	R	E	E	Q	A	E	-	P	D	G	T	E	V	A	D
Human MyHC-embryonic	Y	G	N	M	K	F	K	Q	K	Q	R	E	E	Q	A	E	-	P	D	G	T	E	V	A	D
Human MyHC-2b fast skeletal	Y	G	N	M	K	F	K	Q	K	Q	R	E	E	Q	A	E	-	P	D	G	T	E	V	A	D
Human MyHC-α fast cardiac	Y	G	N	M	K	F	K	Q	K	Q	R	E	E	Q	A	E	-	P	D	G	T	E	D	A	D
Human MyHC-perinatal	Y	G	N	M	K	F	K	Q	K	Q	R	E	E	Q	A	E	-	P	D	G	T	E	V	A	D
Human MyHC-extraocular	Y	G	N	M	K	F	K	Q	K	Q	R	E	E	Q	A	E	-	P	D	G	T	E	V	A	D
Tarantula	L	G	E	M	K	F	K	Q	R	P	R	E	E	Q	A	E	-	A	D	G	T	E	E	G	E
Drosophila melanogaster	M	G	G	M	K	F	K	Q	R	G	R	E	E	Q	A	E	-	Q	D	G	E	E	E	G	G
Caenorhabditis elegans	M	G	N	M	K	F	K	Q	R	P	R	E	E	Q	A	E	-	P	D	G	T	D	E	A	E
Scallop	M	G	E	M	K	F	K	Q	R	P	R	E	E	Q	A	E	-	S	D	G	T	A	E	A	E
Squid	L	G	E	M	K	W	K	-	-	Q	R	G	E	Q	A	E	-	A	D	G	T	A	E	A	E
Non-sarcomeric myosins 2																									
Human NM 2A	L	G	N	I	V	F	K	K	E	R	N	T	D	Q	A	S	M	P	D	N	T	A	A	Q	-
Human NM 2B	F	G	N	I	S	F	K	K	E	R	N	T	D	Q	A	S	M	P	E	N	T	V	A	Q	-
Human NM 2C	F	G	N	I	A	L	K	R	E	R	N	T	D	Q	A	T	M	P	D	N	T	A	A	Q	-
Human Smooth muscle	L	G	N	I	V	F	K	K	E	R	N	T	D	Q	A	S	M	P	D	N	T	A	A	Q	-
Saccharomyces cerevisiae	I	G	N	I	E	I	K	K	T	R	N	D	A	S	L	S	A	D	-	E	P	N	L	K	-
Schizosaccharomyces pombe	M	G	N	I	D	V	G	A	D	R	S	G	-	I	A	R	L	L	N	P	D	E	I	D	-
Dictyostelium	-	G	N	I	K	F	E	K	G	A	G	E	G	A	V	L	-	K	D	K	T	A	L	N	-

Table S1. **Multiple sequence alignment of the loop 4 region of myosin II.**

Residue numbering is based on the bovine β-myosin, MyHC-β (Q9BE39), used in this investigation The Human sarcomeric myosin 2 accession codes are: MyHC-2x – P12882.3, MyHC-2a – NP_060004.3, MyHC-embryonic – NP_002461.2, MyHC-2b – Q9Y623.2, MyHC-α – AAI32668.1, MyHC-β - NP_000248.2, MyHC-perinatal – NP_002463.2, and MyHC-extraocular – NP_003793.2. The Tarantula sequence (UniProt accession code A0A140UGH3_9ARAC) is from *Aphonopelma* used for the cryo-EM structure in Woodhead et al. (1). The *Drosophila melanogaster* sequence (UniProt accession code P05661) is based off of the embryonic isoform structure PDB 5W1A (2). The *C. elegans* sequence (UniProt accession code P12844) is from the myosin-B isoform, with a crystal structure recently obtained (3). The scallop sequence (*Argopecten irradians*) (UniProt accession code P24733) is from myosin structures PDB IDs: 2OTG, 2OS8, 1SR6, 1QVI, 1KK8, and 1S5G. The squid sequence is from the rigor state crystal structure (PDB ID; 3I5G) used to build the homology model in the main text. Human non-muscle and smooth muscle sequence UniProt accession codes are: NM 2A – P35579, NM 2B – P35580, NM 2C – Q7Z406, and smooth muscle – P35749. Sequences for *Saccharomyces cerevisiae*, UniProt P19524, *Schizosaccharomyces pombe*, Q9US16 and *Dictyostelium*, UniProt P08799, myosins are also provided. Grey highlighted residues are residues that are fully or partially conserved, while the arginine group (orange) is conserved amongst the skeletal muscle myosins and appears to shift one position earlier in the non-muscle, smooth muscle and yeast myosins. N.B. Many mammalian non-muscle thin filaments contain tropomyosin, as do yeast thin filaments; no reports identify a *Dictyostelium* tropomyosin and it lacks the highlighted arginine.

Table S2. Data collection and refinement statistics.

Cryo-EM Data Statistics	
Microscope	Titan Krios
Detector	Gatan K2 Summit Direct Detector
Voltage (kV)	300
Magnification	130,000x
Pixel Size (Å)	1.06
Defocus Range (μm)	-1.5 - -2.5
Exposure Times (s/frame)	0.2
Number of Frames (per movie)	35
Total Dose (e^-)	53
Data Processing	
Box Size (pixels)	256
Inter-box Distance (Å)	27.5
Number of Micrographs	2496
Number of Segments after Manual Picking	45,040
Segments after 2D classification	40,455
Segments after 3D classification	32,158
Symmetry Imposed	
Helical Rise (Å)	27.5
Helical Twist (^{o})	166.4
Initial Model	200 Å Featureless Cylinder

Actin-Myosin-Tropomyosin Model Validation	
Atoms	28421 (no hydrogens)
Residues	3555
Ligands	3 Mg^{2+}, 3 ADP
Bonds	
Length (Å)	0.008
Angles (^{o})	1.206
Molprobity Validation	
Molprobity score	2.42
Clash score	23.09
Rotamer Outliers (%)	0.0
Ramachandran Plot	
Outliers (%)	0.26
Allowed (%)	10.29
Favored (%)	89.45
Further Validation	
Resolution Estimation (.143 threshold) (Å)	4.2
Map Sharpening B-Factor ($Å^2$)	-105
Average B-factor ($Å^2$)	70.88

Table S3. Residues along F-actin and myosin S1 that approach each other.

Actin Residue	Residue Atom	Myosin Residue	Residue Atom	Myosin Region	Distance (Å)
TYR337	OH	VAL406	CG1	CM Loop	3.1
VAL30	CG1	VAL406	CG1	CM Loop	3.6
ALA26	CB	VAL404	CG1	CM Loop	3.6
GLU334	OE2	THR412	CB	CM Loop	4.0
TYR337	CE2	THR412	CG2	CM Loop	4.0
ASP24	OD1	LYS405	NZ	CM Loop	4.5
TYR337	OH	TYR410	CD2	CM Loop	4.7
SER350	OG	SER532	OG	Helix-Loop-Helix	3.3
LEU349	CD1	PHE540	CD1	Helix-Loop-Helix	3.5
TYR143	CD1	PRO541	CG	Helix-Loop-Helix	4.0
THR148	CG2	LYS542	CG	Helix-Loop-Helix	4.1
LEU349	CD2	MET539	CB	Helix-Loop-Helix	4.2
THR148	CB	PRO541	CG	Helix-Loop-Helix	4.2
SER350	OG	MET528	CB	Helix-Loop-Helix	4.3
SER348	OG	MET539	CE	Helix-Loop-Helix	4.5
TYR143	CE1	PHE540	CZ	Helix-Loop-Helix	4.6
THR351	CG2	MET528	SD	Helix-Loop-Helix	4.6
THR351	CG2	ILE533	CD1	Helix-Loop-Helix	4.7
MET44	CE	PRO541	CD	Helix-Loop-Helix	4.8
THR351	CG2	LYS551	NZ	Helix-Loop-Helix	4.9
SER350	OG	ILE533	CD1	Helix-Loop-Helix	5.0
THR351	CG2	ASN555	ND2	Helix-Loop-Helix	5.0
ILE330	CD1	GLU371	OE2	Loop 4	3.1
ARG147	NH2	GLU371	CD	Loop 4	3.3

Intermolecular distances are noted for the atoms in actin and myosin residues that approach each other closely (cutoff ≤ 5 Å), based on models fitted to the cryo-EM reconstruction discussed in the main text. Myosin regions located at the actin-myosin interface are named, including the Cardiomyopathy Loop (CM loop), Loop 4, and the Helix-Loop-Helix motif as displayed in Figure 1B (cf. von der Ecken et al., 2016 (4); Fujii and Namba, 2017 (5); Mentes et al., 2018 (6)).

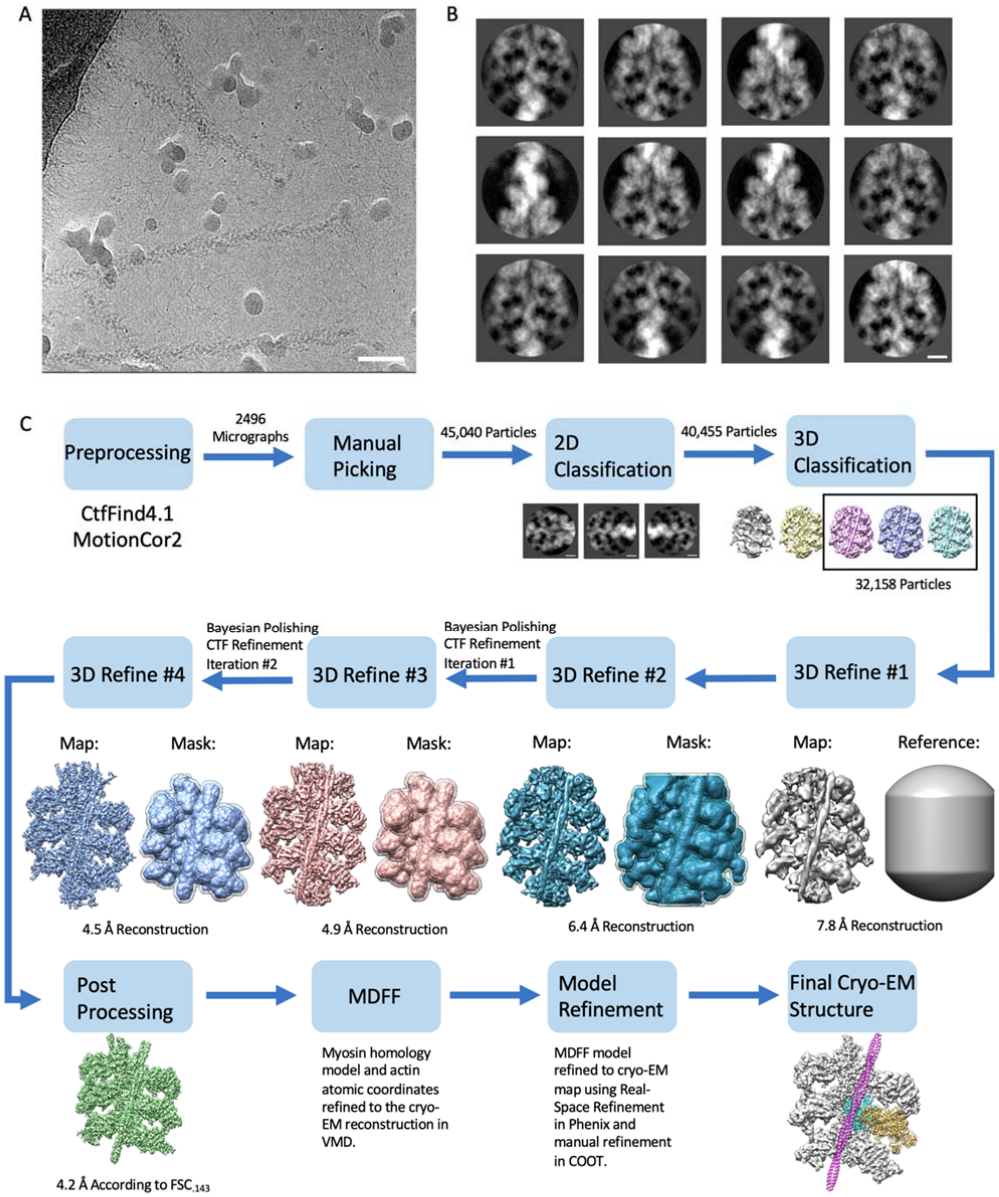

Figure S1. Cryo-EM data processing workflow.

(A) Representative micrograph of myosin S1-decorated actin-tropomyosin filaments frozen in vitreous ice. Unbound tropomyosin and myosin can be seen in the background, well separated from the filaments. Scale bar: 50 nm.

(B) Reference-free two-dimensional class averages of the actin-tropomyosin-myosin S1 segments identified in RELION 3.0.7 (7-9). The actin core of the filament along with myosin S1 arrowheads are visible. Scale bar: 5 nm.

(C) Flowchart describing the cryo-EM workflow performed in RELION 3.0.7 (7-9) that led to the 4.2 Å structure and the pseudo-atomic model of the actin-tropomyosin-myosin S1 complex. This process is also described in detail in the Materials and Methods section in the main text. Micrographs were motion corrected using MotionCor2 and the contrast transfer function (CTF) estimated and normalized by CtfFind4.1. Filaments were manually selected and divided into 270 Å long (256 pixels) overlapping segments, each offset by 27.5 Å (~90% overlap) to produce 45,040 segments. Filament segments were then sorted using two- and three-dimensional classification. Noisy or poorly defined segments were discarded. In all routines done in three-dimensions, F-actin helical symmetry was applied (166.4° subunit rotation around the F-actin helical axis and a subunit axial translation of 27.5 Å). A final set of 32,158 segments was taken for a preliminary three-dimensional refinement by first aligning these particles to a featureless 200 Å diameter cylinder, generating a 7.8 Å reconstruction. The resulting model was low-pass filtered to 60 Å to be used as a new reference for a second refinement while incorporating a solvent mask to produce a subsequent reconstruction at 6.4 Å. Two iterations of Contrast Transfer Function (CTF) refinement and Bayesian "Polishing" were then performed. Particles underwent CTF refinement with beam tilt estimation and a subset of these particles was evaluated to find optimal polishing parameters. After polishing, the optimized particles were used in the next refinement using the 6.4 Å reconstruction low-pass filtered to 60 Å as a starting model. An additional soft 6 actin-6 myosin-tropomyosin mask was employed after each iteration to focus the refinement on the central section of the acto-S1 filaments. The first iteration of CTF refinement and Bayesian polishing process re[Myosin homology model and actin atomic coordinates Refined to the cryo-EM reconstruction in VMD.] 4.9 Å resolution map. The same process was repeated once [duce a final 4.5 Å resolution map. Further iterations did not in[resolution. Final resolution estimation was made using Fourier [ation criteria, ($FSC_{0.143}$) in the RELION post processing step, wh[d a final 6-actin-6-myosin-tropomyosin map at 4.2 Å. This map was used in initial MDFF flexible fitting (10) to match a myosin homology model and F-actin model to experimental density. Refinements in PHENIX (11) and Coot (12) produced the final actomyosin

structure (see Materials and Methods section). An idealized tropomyosin coiled coil was then fitted into the density.

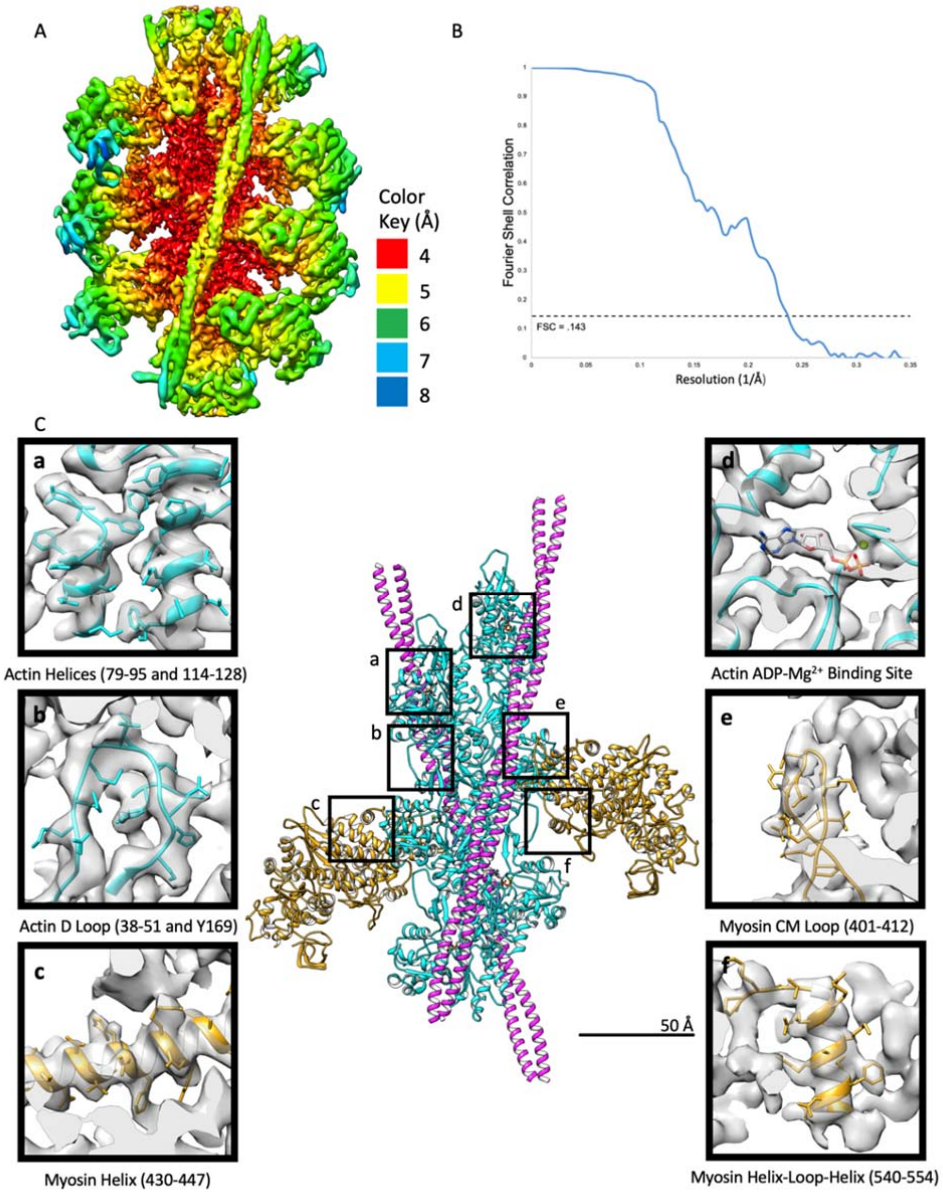

Figure S2. Local resolution of components of the reconstruction.

A. Heat map visualization showing resolution values of locally filtered data comprising the actin-tropomyosin-S1 reconstruction, calculated with the LocalRes sub-routine in RELION 3.0.7 (7-9). Actin displays the highest resolution extending to 4.0 Å, the actin-myosin interface averages a resolution of 4.5 Å, tropomyosin ranges between 5 to 6.5 Å resolution limits and the distal regions of myosin are upwards of 6 to 7 Å resolution.

B. Fourier Shell Correlation (FSC) plot of the reconstruction following final processing in RELION 3.0.7 (7-9). The calculated $FSC_{0.143}$ of 0.238 $Å^{-1}$ corresponds to a global resolution of 4.2 Å.

C. Atomic models fitted to the cryo-EM density. Selected regions of the actin-myosin complex were picked and reoriented to better display the model to map correspondence.

Figure S3. Myosin-induced sliding of tropomyosin on actin.

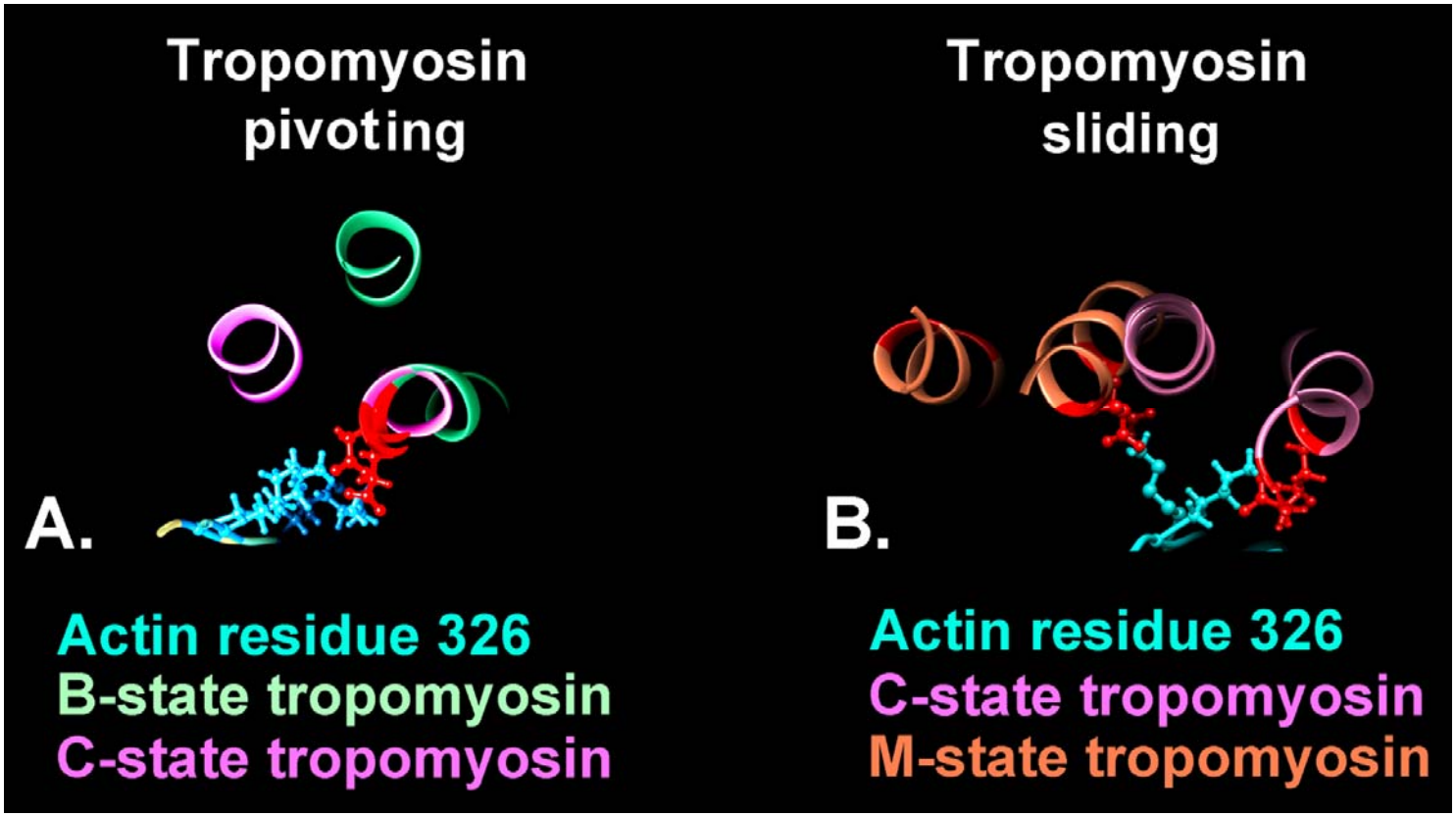

A. **B-state to C-state transition**. Superimposed transverse sections through B-state and C-state poses of the Pavadai et al. models of the thin filament (13) made at residue 326 (cyan) of actin on tropomyosin pseudo-repeat 4, showing electrostatic contacts between actin Lys326 and Glu138 of tropomyosin. Note the electrostatic contacts are between actin and the closest α-helical chain of the tropomyosin coiled coil; this chain is relatively stationary for the B/C-state transition, while the outer chains pivot between B- and C-states. Such tropomyosin pivoting characterizes the B-state/C-state transition over all pseudo-repeats except at the tropomyosin overlapping domain (13,14). Figure made from data in (13).

B. **C-state to M-state transition**. Superimposed transverse sections through C-state and M-state poses comparing the Pavadai et al. C-state model (13) and the M-state model determined in the current work, again made through residue 326 (cyan) of actin on tropomyosin pseudo-repeat 4, showing electrostatic contacts between actin Lys326 and Glu138 of C-state tropomyosin and Lys326 to Glu142 of M-state tropomyosin. Once more, electrostatic contact is made between actin and the closest of the α-helical chains of tropomyosin, but here tropomyosin pivoting is not observed and, instead, pure azimuthal sliding of the coiled coil takes place during the C/M-state transition. In fact, it is now the sidechain of Lys326 that pivots. For simplicity, the position of myosin-S1 is not shown for the M-state.

REFERENCES

1. Woodhead, J.L., F.Q. Zhao, R. Craig, E.H. Egelman, L. Alamo, and R. Padrón. 2005. Atomic model of a myosin filament in the relaxed state. *Nature.* 436:1195-1199.
2. Cadwell, J.T., D.J. Mermelstein, R.C. Walker, S.I. Berstein, and T. Huxford. 2019. X-ray crystallography and molecular dynamics analysis of Drosophia melanogaster embryonic muscle myosin define domains responsible for isoform-specific properties. *J. Mol. Biol.* 432:427-447.
3. Hellerschmied, D., A. Lehner, N. Franicevic, R. Arnese, C. Johnson, A. Vogel, A. Meinhart, R. Kurzbauer, L. Deszcz, L. Gazda, M. Geeves, and T. Clausen. 2019. Molecular features of the UNC-45 chaperone critical for binding and folding muscle myosin. *Nature Commun*. 10:4781.
4. von der Ecken J., S.M. Heissler, S. Pathan-Chhatbar, D.J Manstein, and S. Raunser. 2016. Cryo-EM structure of a human cytoplasmic actomyosin complex at near-atomic resolution. *Nature*. 534:724-728.
5. Fujii, T, and K. Namba. 2017. Structure of actomyosin rigour complex at 5.2 Å resolution and insights into the ATPase cycle mechanism. *Nat. Commun*. 2017 8:13969.
6. Mentes, A., A. Huehn, X. Liu, A. Zwolak, R. Dominguez, H. Shuman, E.M. Ostap, and C.V. Sindelar. 2018. High-resolution cryo-EM structures of actin-bound myosin states reveal the mechanism of myosin force sensing. *Proc. Natl. Acad. Sci. USA*. 115:1292-1297.
7. Scheres, S.H. 2012. RELION: implementation of a Bayesian approach to cryo-EM structure determination. *J. Struct. Biol*. 180:519-530.
8. Scheres, S.H. 2016. Processing of structurally heterogeneous Cryo-EM aata in RELION. *Methods Enzymol*. 579:125-157.
9. He, S, and S.H.W Scheres. 2017 Helical reconstruction in RELION. *J. Struct. Biol.* 198:163-176.
10. Trabuco, L.G., E. Villa, E. Schreiner, C.B. Harrison, and K. Schulten. 2009. Molecular dynamics flexible fitting: A practical guide to combine cryo-electron microscopy and x-ray crystallography. *Methods*. 49:174-180.
11. Afonine, P.V., B.K. Poon, R.J. Read, O.V.Sobolev, T.C. Terwilliger, A. Urzhumtsev, and P.D. Adams. 2018. Real-space refinement in PHENIX for cryo-EM and crystallography. *Acta Crystallogr. D Struct. Biol*. 74:531-544.
12. Emsley, P., B. Lohkamps, W.G. Scott, and K. Cowtan. 2010. Features and development of Coot. *Acta Crystall. D Struct. Biol.* 66: 486-501.
13. Pavadai, E., W. Lehman, and M.J. Rynkiewicz. 2020. Protein-protein docking reveals dynamic interactions of tropomyosin on actin filaments. *Biophys. J.* 119: 77-86.
14. Yamada, Y., K. Namba, and T. Fujii. 2020. Cardiac Muscle thin filament structures reveal calcium regulatory mechanism. *Nature Commun*. 11:153.